World Academy of Science, Engineering and Technology
International Journal of Geological and Environmental Engineering
Vol:11, No:9, 2017

Rapid Monitoring of Earthquake Damages Using Optical and SAR Data

Saeid Gharechelou, Ryutaro Tateishi

***Abstract*—**Earthquake is an inevitable catastrophic natural disaster. The damages of buildings and man-made structures, where most of the human activities occur are the major cause of casualties from earthquakes. A comparison of optical and SAR data is presented in the case of Kathmandu valley which was hardly shaken by 2015-Nepal Earthquake. Though many existing researchers have conducted optical data based estimated or suggested combined use of optical and SAR data for improved accuracy, however finding cloud-free optical images when urgently needed are not assured. Therefore, this research is specializd in developing SAR based technique with the target of rapid and accurate geospatial reporting. Should considers that limited time available in post-disaster situation offering quick computation exclusively based on two pairs of pre-seismic and co-seismic single look complex (SLC) images. The InSAR coherence pre-seismic, co-seismic and post-seismic was used to detect the change in damaged area. In addition, the ground truth data from field applied to optical data by random forest classification for detection of damaged area. The ground truth data collected in the field were used to assess the accuracy of supervised classification approach. Though a higher accuracy obtained from the optical data then integration by optical-SAR data. Limitation of cloud-free images when urgently needed for earthquak evevent are and is not assured, thus further research on improving the SAR based damage detection is suggested. Availability of very accurate damage information is expected for channelling the rescue and emergency operations. It is expected that the quick reporting of the post-disaster damage situation quantified by the rapid earthquake assessment should assist in channeling the rescue and emergency operations, and in informing the public about the scale of damage.

***Keywords*—**Sentinel-1A data, Landsat-8, earthquake damage, InSAR, rapid monitoring, 2015-Nepal earthquake.

I. Introduction

THE concentration of population in urban areas is rapidly increasing and earthquake is one of the most catastrophic natural disasters for them. The technically sound cities with earthquake-resistant infrastructures and prompt emergency services can defend damages from large earthquakes; whereas rampant buildings in vulnerable fault zones are perils of mass deaths and cremations. The extravagant deaths and injuries due to earthquakes observed over last few decades undermine present urbanization. While urbanization is inevitable at the expense of rising population, damage reduction strategies in earthquake-prone regions are mandatory. Though earthquakes are unavoidable, their damages can be minimized by disaster preparedness and tactful management.

Saeid Gharechelou is with the Faculty of Civil Engineering, Shahrood University of Technology, Shahrood, Iran (e-mail: sgharachelo@gmail.com).

Ryutaro Tateishi is with the Center for Environqwmental Remote Sensing (CEReS), Chiba University, Japan.

Earthquakes have caused more than 23 million deaths during the period of 1902-2011 alone globally [1]. Nepal is one of the most earthquake-prone countries in the world. The geodetic strain emerged on Main Himalayan Thrust (MHT) fault and potential seismic hazard across Nepal Himalaya has been well described by scientists [2]-[12]. In line with this, an earthquake with a moment magnitude (M_W) of 7.8 occurred on April 25, 2015 followed by another major aftershock with 7.3 M_W on May 12, 2015, and hundreds of large aftershocks after that. This earthquake occurred as the result of thrust faulting on or near the MHT between the subducting India plate and the overriding Eurasia plate at a rate of 45 mm per year to the north [1]. It causes more than 9,000 deaths, 23,000 injured, 500,000 families homeless, and 2.8 million people in need of humanitarian assistance [13]. The sequence of major aftershocks also triggered thousands of landslides in the steep topography of Nepal with hundreds of fatalities and road blocks to the villages [14].

Nepal has an evidence of 17 earthquakes larger than 6.0 M_W in the documented history since 1225 [1]. The 1225-earthquake as the first recorded earthquake in Nepal believed to have killed one-third of the total population in Kathmandu including the king of Nepal; the earthquakes of 1408, 1505, 1681, 1767, 1833, and 1916 were said to have as devastating as of 1225. The 8.4 M_W earthquake of 1934 was very destructive which killed 8,519 people's lives. The terrifying moment of this earthquake has been well described by Rana, 1935. The 2015-earthquake was the worst natural disaster Nepal faced since 1934. Scientists have indicated that more calamitous mega earthquake appears to be inevitable to Nepal's future because the present earthquakes have failed to fully rupture the main fault beneath the Himalaya [15]-[17]. These scientific statements urge that Nepal requires boosting up its disaster preparedness plan.

Buildings damage information is essential for rescue, humanitarian and reconstruction operations in the disaster area [18]. The satellite-based optical and SAR data have been used for buildings damage assessment after major earthquakes in a number of places, for example 1995-earthquake in Kobe, Japan [19], 1999-earthquake in Izmit, Turkey [20], 2001-earthquake in Gugrat, India [21], [22], 2003-earthquake in Bam, Iran [23]-[26], 2005-earthquake in Azad Kasmir, Pakistan [27], 2006-earthquake in Java, Indonesia [28], 2008-earthquake in Sichuan, China [29]-[32], 2009-earthquake in L'Aquila, Italy [33], [34], and 2010-earthquake in Haiti [35]-[37].

Different techniques have been utilized for retrieving the earthquake-induced buildings damage information from

remotely sensed imagery such as very high resolution satellite imagery [38]-[40], stereo photographs [41], [42], combination of SAR and optical data [43], [44], object based identification [45], [46], supervised classification [47], [48], airborne imagery [49]-[51], SAR backscattering intensity [52], [53], Multi-temporal SAR images [54], unmanned aerial vehicle images [55], [56], template matching and pattern recognition [57], and textural and the spectral features [58], [59]. Buildings damage is often measured by grading the level of damages, e.g., heavy damage, moderate damage, and low damage [60]-[63]. However, detection of lower damage levels is challenging while the remotely sensed images are mostly capable of detecting heavy damage levels, i.e., totally collapsed buildings [64], [65]. After the 2015-Nepal earthquake, reconnaissance survey of the damaged buildings and structures have been conducted by some researchers and reported the damage to poorly structured stone/brick masonry buildings, subsidence of soft soils and lateral spreading [66]-[69].

The importance of near real-time disaster mapping using satellite data to minimize the effects of natural disasters have been discussed [70]. The major hazards caused by the earthquakes are ground shaking, ground displacement, soil liquefaction, and flooding/tsunami. All these hazards can seriously damage buildings where most of the human activities occur. The quick reporting of the post-disaster damage situation is necessary for channelling the rescue and emergency operations, and in informing the public about the scale of damage. Satellite with a capacity of repeat observation and wide area coverage offers optical and synthetic aperture radar (SAR) data applicable to damage detection. Though many attempts have been made for the satellite based detection of damages, accuracy is an issue immensely important. This research aims to increase the accuracy of detection of buildings damaged by mining important features from optical and SAR data through supervised learning approach, and discuss potentialities of the selected features.

II. Methodology

A. Study Area

This research was carried out in the urban areas of the Kathmandu valley which was severely hit by the 2015-Nepal earthquake. The Kathmandu valley is the bowl-shaped valley standing at 1,425 meters above sea level surrounded by mountainous ranges. It consists of several cities and villages including Kathmandu metropolitan city, the capital of Nepal. This valley as a lake in geological past has faced big earthquakes throughout the history. The valley is a cultural and economic hub of Nepal hosting several world heritage sites. The location map of the study area is displayed in Fig. 1. The major shake areas are also shown in Fig. 1 based on Mercalli intensity data of the earthquake [1] which demonstrates that the Kathmandu valley was severely shaken.

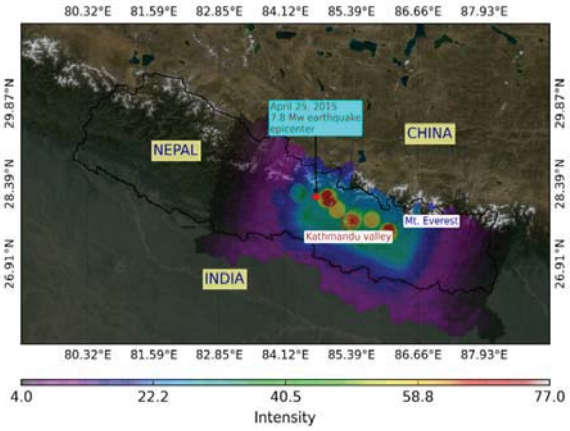

Fig. 1 Location map of the study area, the Kathmandu valley, Nepal (red polygon) along with the epicenter and major shake areas

B. Processing of the Satellite Data

Sentinel-1 mission by European Space Agency (ESA) provides free data from a C-band Synthetic Aperture Radar (SAR) instrument from April 2014. We used the pre-seismic and post-seismic images in VH and VV polarizations from the Sentinel-1 Ground Range Detected (GRD) product. The GRD product consists of focused SAR data that has been detected, multi-looked and projected to the ground range using an Earth ellipsoid model. The resulting product has approximately square resolution pixel by 13 m and square pixel spacing. We processed the GRD scenes using the Sentinel-1 Toolbox available freely from the ESA to generate a calibrated and terrain-corrected product. The final terrain corrected images were converted to decibels via log scaling and quantized to 16-bits. For change detection, we calculated the ratio between post-seismic and pre-seismic polarizations (VH and VV). We also calculated 18 types of image textures using the gray-level co-occurrence matrix (GLCM) functions using 3×3 sliding window size with a single pixel offset. Then, the ratios between post-seismic and pre-seismic textures were calculated for supervised learning.

We also calculated pre-seismic and co-seismic phase coherence from Sentienel-1 Single Look Complex (SLC) product using Interferometry Synthetic Aperture Radar (InSAR) technique. The SLC product consists of focused SAR data geo-referenced using orbit and attitude data from the satellite and provided in zero-Doppler slant-range geometry. The InSAR technique uses phase difference between two observations taken from slightly different sensor positions. Two pairs of SLC images representing pre-seismic (March 24, 2015 and April, 17) and co-seismic (April 17, 2015 and April 29, 2015) events were co-registered and coherence were calculated using Sentinel-1 Toolbox. The terrain corrected coherence images were used to calculate the ratio between co-seismic and pre-seismic coherences as an additional feature for the change detection. We also calculated post-seismic (April 29, 2015 and May 11, 2015) coherence image to compare the phase change after and before the earthquake. It should be noted that the post-seismic pair uses the SLC images taken before large aftershock on May 12, 2015. The

perpendicular (temporal) baseline differences of the co-seismic and pre-seismic image pairs were 38.92 meters (12-days), and -34.82 meters (24-days) respectively as minor differences for damage detection.

The standard terrain corrected (Level 1T) Landsat 8 Operational Land Imager (OLI) and Thermal Infrared Sensor (TIRS) scenes belonging to pre-seismic and post-seismic events were processed. The Digital Numbers (DNs) for each OLI and TIRS band delivered as 16-bit unsigned integers were converted into Top-Of-Atmosphere (TOA) spectral reflectance and brightness temperature (K) values using the rescaling coefficients found in the metadata file. Out of nine OLS and two TIRS bands of the Landsat 8 data, seven bands (blue, green, red, near infrared, mid infrared shortwave infrared and thermal infrared) were extracted. The clouds were removed by using separate Quality Assessment (QA) band information available in the Landsat 8 data. The ratios of post-seismic and pre-seismic images of all seven Landsat 8 bands were calculated. 18 types of image textures for each band were calculated for each of the post-seismic and pre-seismic images. Then, the ratio between the post-seismic and pre-seismic textures were also calculated. Altogether, a stack of 172 feature images was prepared from the Sentinel-1, Landsat 8 data, and used in the research. The input feature images are listed out in Table I.

C. Collection of the Ground Truth Data

For evaluating the strength of earthquake impacts to a specific place, the European Macro-seismic Scale [72] has used twelve damage scales. For rapid monitoring of earthquake damages using satellite data, discriminating all the twelve damage scales are not only difficult but also not necessary. Therefore, from satellite perspectives, the EMS scales are summarized into three damage levels in our research as follows: safe, danger, and lethal.

1. Safe: Divisions 1-3 (not felt, scarcely felt, weak, and largely observed) including not felt by everyone, felt by individual indoor peoples, noticeable shaking of many objects and swing of hanging objects respectively without any damage to the buildings are termed as safe to the peoples nearby.
2. Danger: Divisions 4-7 (strong, slightly damaging, and damaging) including the toppling of heavy objects, falling of objects on wall, and shifted furniture and falling of objects from the shelves respectively that can kill and injure the peoples are termed as “danger”, but they cannot be discriminated by satellite images and did not account.
3. Lethal: Divisions 8-12 (heavily damaging, destructive, very destructive, devastating, and completely devastating) including the partial collapse of few buildings, partial collapse of many buildings, the collapse of many buildings, the collapse of most buildings, and destruction of all structures respectively are termed as lethal damages.

After 2015- earthquake in Nepal, locations of the lethal and safe damages were collected through visual inspection in the field. The polygon around the lethal and safe blocks as seen on the ground was recorded based on a GPS instrument. Not only the residential buildings but also the public buildings, historical monuments, towers, and temples were included. However, the brick walls in the periphery of houses which were damaged elsewhere were not accounted. Altogether 105 polygons belonging to each class were collected. The distribution of the ground truth polygons are plotted in Fig. 2.

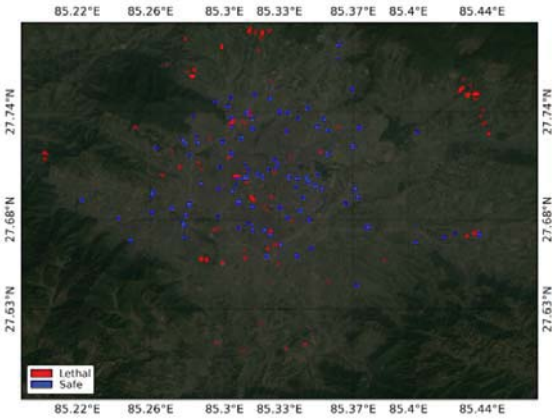

Fig. 2 Distribution of the ground truth polygons in the Kathmandu valley displayed over Landsat-8 based RGB composite image

TABLE I
LIST OF 172 INPUT FEATURES USED IN THE RESEARCH

Features	Landsat 8	Sentinel-1
Post-seismic and pre-seismic optical bands ratio	7	-
Post-seismic and pre-seismic optical textures ratio	7 ×18	-
Post-seismic and pre-seismic SAR polarizations ratio	-	2
Post-seismic and pre-seismic SAR textures ratio	-	2 ×18
Post-seismic and co-seismic InSAR coherence ratio	-	1
Sub-total	133	39
Total		172

D. Supervised Classification and Accuracy Analysis

The mean pixel values of 172 feature images were calculated for each of the ground truth polygons, and supervised classification approach was used for the detection of buildings damages. The Random Forests algorithm that uses bootstrap aggregating (bagging) to form an ensemble of trees by searching random subspaces from the given data (features) and the best splitting of the nodes by minimizing the correlation between the trees, was used as a supervised classifier [71]. Out of 110 polygons belonging to each class, 55 polygons were used for training the Random Forests model, whereas remaining 55 polygons were used for analyzing the accuracy of the model. The hierarchy of best features provided by the random forests algorithm was used to identify the importance of features through assessment of each subset of features separately. The overall accuracy and kappa coefficient were used as the metrics of accuracy.

III. RESULTS AND DISCUSSION

A. Visualization of the Lethal Blocks

The time-lapse images from very high resolution satellite data are vital information for grasping quick geospatial information of the disaster situation and assessing the scale

and extent of damages. Google Earth can be a useful platform for quick delivery of the damage information due to its free accessibility mainly for countries which lack modern data infrastructure. Examples of the lethal block polygons as collected in the field have been demonstrated in Fig. 3 using pre-seismic and post-seismic Google Earth images. In each location in Fig. 3, the scale and extent of damages are clearly distinguished which confirms the suitability of Google Earth images for rapid damage assessment if promptly updated soon after the availability of very high resolution images.

Fig. 3 Examples of the lethal blocks (red polygons) as collected in the field using pre-seismic (left) and post-seismic (right) Google Earth images

B. Coherence Changes

The coherence is the complex cross-correlation coefficient of the SAR image pair, provides the similarity between the pre-event and post-event images after compensating the topographic phase. The phase coherence as computed from the pair of pre-seismic, co-seismic, and post-seismic images have been shown in Fig. 4. The coherence images obtained from each pair have provided larger coherence over buildings and man-made structures, whereas forests, croplands, and water bodies provided lower coherence. However, there was a strong drop of the co-seismic coherence (Fig. 4 (b)) as compared to pre-seismic (Fig. 4 (a)) and post-seismic coherence (Fig. 4 (c)), which provides qualitative information about the earthquake induced damages. The red colour shows more change and damage by value range of coherence change.

C. Detection of Buildings Damage

The accuracy of the detection of the building's damages was analysed using the overall accuracy and kappa coefficient. The kappa coefficient measures inter-rater agreement for categorical variables by counting the proportion of instances that predictions agreed with the validation data (observed accuracy), after adjusting for the proportion of agreements taking place by chance (expected accuracy) [73].

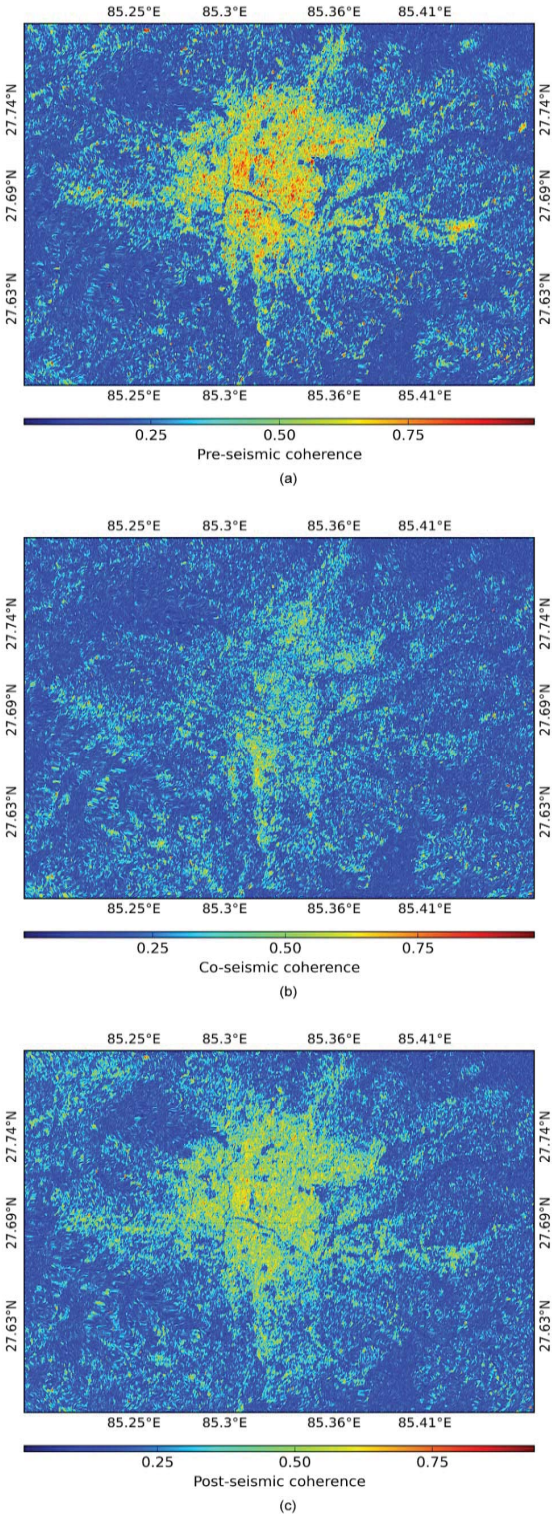

Fig. 4 A large drop of the co-seismic coherence (b) as compared to pre-seismic (a) and post-seismic (c) coherence

A fifty percent of the sample polygons collected in the field were used for the calculation of overall accuracy and kappa coefficient which were not used for fitting the Random Forests model. The variation of the overall accuracy and kappa coefficient with respect to the combinations of the features is displayed in Fig. 5. The maximum accuracy (Overall accuracy = 0.92, Kappa coefficient = 0.84) could be obtained by the combination of 94 features. The best performed 87 features belong to the SAR, optical and textural data sources.

The performance of each dataset for the detection of buildings damages are also summarized in Table II. The SAR group (HV and VV polarizations, their 18 types of textures, and co-seismic/pre-seismic coherence) provided overall accuracy and kappa coefficient of 0.83 and 0.66 respectively which is lower than the optical group based accuracy (overall accuracy (0.92), kappa coefficient (0.84). Nevertheless, a combination of the SAR based features with the optical data did not improve the accuracy more than provided by the optical data based features.

This accuracy based analysis suggested that optical data mainly the very-high-resolution imageries are more important than the SAR data for the detection of buildings damages. However, time is a determining factor for the quick reporting of the building's damages in the aftermath of disasters. The availability of optical data as determined by clouds and atmospheric conditions cannot be guaranteed in that short period. Therefore, SAR data are the most important for the detection of buildings damaged. However, accuracy of the SAR data is not very high, kappa coefficient is 0.66 which is more important than overall accuracy, therefore future research should focus on increasing the accuracy of the SAR based buildings damages detection.

The comparison of the co-seismic coherence image with the pre-seismic and/or post-seismic coherence images showed very clear qualitative information on the scale and extent of the earthquake damages. It is very useful information for rapid assessment of the severity the earthquake damages. However, tracking individual damaged buildings is very challenging solely using the coherence data. Many houses in Kathmandu are surrounded by walls which are just stacks of bricks glued together with a little concrete which are highly prone to damage even by small-scale earthquakes. Since the SAR data are very sensitive to the surface changes, the wall damages provide false alarm on the detection of lethal damages. It is expected that the availability of sub-meter resolution SAR data in future could provide buildings level changes with high accuracy.

TABLE II
PERFORMANCE OF RANDOM FORESTS ALGORITHM FOR THE DETECTION OF BUILDINGS DAMAGES

Features (Number of features)	Overall accuracy (Kappa coefficient)	Optimum features
Sentinel-1 only	0.83 (0.66)	33
Landsat-8 only	0.92 (0.84)	21
Sentinel-1& Landsat	0.92 (0.84)	94

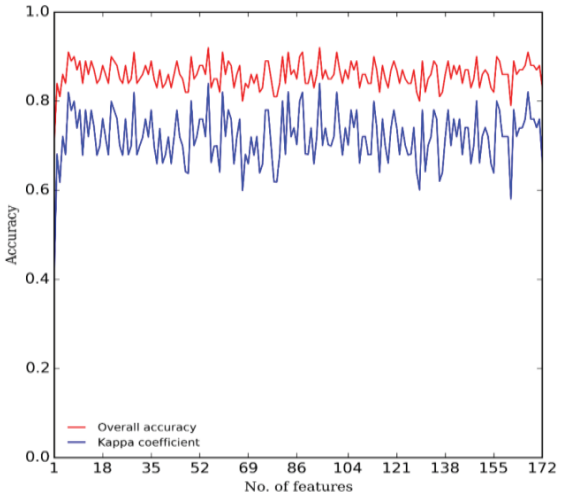

(a)

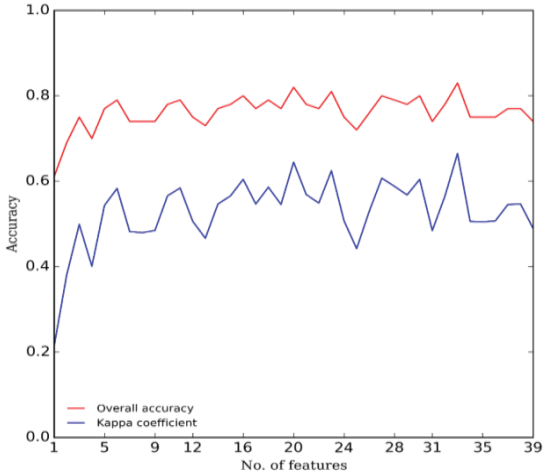

(b)

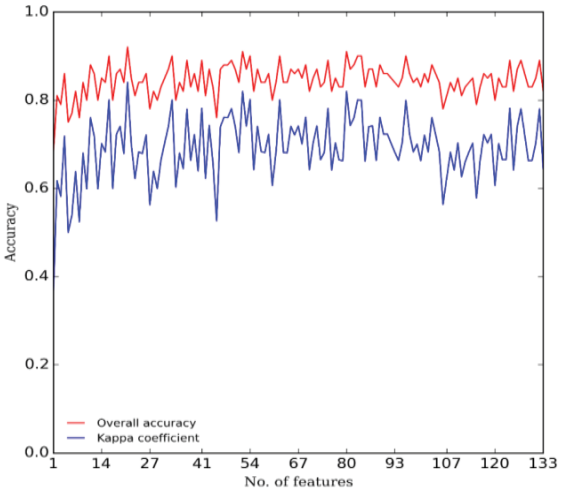

(c)

Fig. 5 (a) Performance of the SAR plus optical features (Sentinel-1 and Landsat 8) for the detection of buildings damages, (b) SAR features (Sentinel-1) only and (c) optical features only (Landsat 8)

IV. Conclusion

Since the available time is hurdling for the post-disaster situation, a suitable method for the rapid geospatial reporting of the earthquake-induced damages was presented in this research. Though the optical data provided more accurate damage detection with using of three division of ground truth data collecting and integration with SAR data can work for improving the accuracy of building damage. In this way finding cloud-free optical images when urgently needed are not assured, future research on increasing the accuracy of SAR data that works even in the case of clouds and rains is suggested. However, by changing the coherence SAR data can observe the damage of buildings but, this change may cause of other resaon as well, therefore investigation and combination with optical data and filed data can help to improve the accuracy. On the other hand, some researchers used the backscatter from SAR data for detecting the change and damage of buildings while this change in backscatter is coming up by different sources from a ground object such as moisture contents and chemical variation of materials. In this was using the coherence change would be the best way to detecting the change.

Acknowledgements

The authors are thankful to Dr. Ram C. Sharma for great help for data processing and editing the manuscript.

References

[1] USGS-Earthquakes. (2015, October 03). Available: http://earthquake.usgs.gov/earthquakes
[2] R. Bilham, "Location and magnitude of the 1833 Nepal earthquake and its relation to the rupture zones of contiguous great Himalayan earthquakes," Current Science, vol. 69, pp. 101-128, 1995.
[3] R. Bilham, "Seismology: Raising Kathmandu," Nature Geosci, vol. 8, pp. 582-584, 2015.
[4] R. Bilham, K. Larson, and J. Freymueller, "GPS measurements of present-day convergence across the Nepal Himalaya," Nature, vol. 386, pp. 61-64, 1997.
[5] R. Cattin and J. P. Avouac, "Modeling mountain building and the seismic cycle in the Himalaya of Nepal," Journal of Geophysical Research: Solid Earth, vol. 105, pp. 13389-13407, 2000.
[6] J. Lavé, D. Yule, S. Sapkota, K. Basant, C. Madden, M. Attal, et al., "Evidence for a Great Medieval Earthquake (~1100 A.D.) in the Central Himalayas, Nepal," Science, vol. 307, pp. 1302-1305, 2005.
[7] T. Ader, J.-P. Avouac, J. Liu-Zeng, H. Lyon-Caen, L. Bollinger, J. Galetzka, et al., "Convergence rate across the Nepal Himalaya and interseismic coupling on the Main Himalayan Thrust: Implications for seismic hazard," Journal of Geophysical Research: Solid Earth, vol. 117, pp. 2012.
[8] J. L. Mugnier, A. Gajurel, P. Huyghe, R. Jayangondaperumal, F. Jouanne, and B. Upreti, "Structural interpretation of the great earthquakes of the last millennium in the central Himalaya," Earth-Science Reviews, vol. 127, pp. 30-47, 2013.
[9] L. Bollinger, S. N. Sapkota, P. Tapponnier, Y. Klinger, M. Rizza, J. Van der Woerd, et al., "Estimating the return times of great Himalayan earthquakes in eastern Nepal: Evidence from the Patu and Bardibas strands of the Main Frontal Thrust," Journal of Geophysical Research: Solid Earth, vol. 119, pp. 7123-7163, 2014.
[10] V. L. Stevens and J. P. Avouac, "Interseismic coupling on the main Himalayan thrust," Geophysical Research Letters, vol. 42, pp. 5828-5837, 2015.
[11] J.-P. Avouac, "Mountain building, erosion, and the seismic cycle in the Nepal Himalaya" in Advances in Geophysics. vol. Volume 46, ed: Elsevier, 2003, pp. 1-80.
[12] J.-P. Avouac, L. Meng, S. Wei, T. Wang, and J.-P. Ampuero, "Lower edge of locked Main Himalayan Thrust unzipped by the 2015 Gorkha earthquake," Nature Geosci, vol. 8, pp. 708-711, 2015.
[13] UNOCHA, "UN Office for the Coordination of Humanitarian Affairs," 2015.
[14] B. D. Collins and R. W. Jibson, "Assessment of existing and potential landslide hazards resulting from the April 25, 2015 Gorkha, Nepal earthquake sequence," Reston, VA, Report 2015-1142, 2015.
[15] Bilham, Roger. 2015. “Seismology: Raising Kathmandu.” Nature Geosci 8: 582–584.
[16] E. Hand and P. Pulla, "Nepal disaster presages a coming megaquake," Science, vol. 348, pp. 484-485, 2015.
[17] J. E. Harvey, D. W. Burbank, and B. Bookhagen, "Along-strike changes in Himalayan thrust geometry: Topographic and tectonic discontinuities in western Nepal," Lithosphere, vol. 7, pp. 511-518, 2015.
[18] L. Dong and J. Shan, "A comprehensive review of earthquake-induced building damage detection with remote sensing techniques," ISPRS Journal of Photogrammetry and Remote Sensing, vol. 84, pp. 85-99, 2013.
[19] M. Matsuoka and F. Yamazaki, "Use of Satellite SAR Intensity Imagery for Detecting Building Areas Damaged Due to Earthquakes," Earthquake Spectra, vol. 20, pp. 975-994, 2004.
[20] M. Turker and B. T. San, "SPOT HRV data analysis for detecting earthquake-induced changes in Izmit, Turkey," International Journal of Remote Sensing, vol. 24, pp. 2439-2450, 2003.
[21] Y. Yusuf, M. Matsuoka, and F. Yamazaki, "Damage assessment after 2001 Gujarat earthquake using Landsat-7 satellite images," Journal of the Indian Society of Remote Sensing, vol. 29, pp. 17-22, 2001.
[22] K. Saito, R. J. S. Spence, C. Going, and M. Markus, "Using High-Resolution Satellite Images for Post-Earthquake Building Damage Assessment: A Study Following the 26 January 2001 Gujarat Earthquake," Earthquake Spectra, vol. 20, pp. 145-169, 2004.
[23] G. A. Arciniegas, W. Bijker, N. Kerle, and V. A. Tolpekin, "Coherence- and Amplitude-Based Analysis of Seismogenic Damage in Bam, Iran, Using ENVISAT ASAR Data," Geoscience and Remote Sensing, IEEE Transactions on, vol. 45, pp. 1571-1581, 2007.
[24] P. Gamba, F. Dell'Acqua, and G. Trianni, "Rapid Damage Detection in the Bam Area Using Multitemporal SAR and Exploiting Ancillary Data," Geoscience and Remote Sensing, IEEE Transactions on, vol. 45, pp. 1582-1589, 2007.
[25] J. Hoffmann, "Mapping damage during the Bam (Iran) earthquake using interferometric coherence," International Journal of Remote Sensing, vol. 28, pp. 1199-1216, 2007/03/20 2007.
[26] M. Chini, N. Pierdicca, and W. J. Emery, "Exploiting SAR and VHR Optical Images to Quantify Damage Caused by the 2003 Bam Earthquake," Geoscience and Remote Sensing, IEEE Transactions on, vol. 47, pp. 145-152, 2009.
[27] M. Chini, F. R. Cinti, and S. Stramondo, "Co-seismic surface effects from very high resolution panchromatic images: the case of the 2005 Kashmir (Pakistan) earthquake," Nat. Hazards Earth Syst. Sci., vol. 11, pp. 931-943, 2011.
[28] H. Miura, S. Midorikawa, and N. Kerle, "Detection of Building Damage Areas of the 2006 Central Java, Indonesia, Earthquake through Digital Analysis of Optical Satellite Images," Earthquake Spectra, vol. 29, pp. 453-473, 2013.
[29] D. Ehrlich, H. D. Guo, K. Molch, J. W. Ma, and M. Pesaresi, "Identifying damage caused by the 2008 Wenchuan earthquake from VHR remote sensing data," International Journal of Digital Earth, vol. 2, pp. 309-326, 2009/12/01 2009.
[30] T. Balz and M. Liao, "Building-damage detection using post-seismic high-resolution SAR satellite data," International Journal of Remote Sensing, vol. 31, pp. 3369-3391, 2010.
[31] D. Brunner, G. Lemoine, and L. Bruzzone, "Earthquake Damage Assessment of Buildings Using VHR Optical and SAR Imagery," Geoscience and Remote Sensing, IEEE Transactions on, vol. 48, pp. 2403-2420, 2010.
[32] G. Pan and D. Tang, "Damage information derived from multi-sensor data of the Wenchuan Earthquake of May 2008," International Journal of Remote Sensing, vol. 31, pp. 3509-3519, 2010.
[33] F. Dell'Acqua, C. Bignami, M. Chini, G. Lisini, D. A. Polli, and S. Stramondo, "Earthquake Damages Rapid Mapping by Satellite Remote Sensing Data: L'Aquila April 6th, 2009 Event," Selected Topics in Applied Earth Observations and Remote Sensing, IEEE Journal of, vol. 4, pp. 935-943, 2011.
[34] F. Dell'Acqua and P. Gamba, "Remote Sensing and Earthquake Damage Assessment: Experiences, Limits, and Perspectives," Proceedings of the

IEEE, vol. 100, pp. 2876-2890, 2012.
[35] C. Corbane, K. Saito, Dell, L. Oro, E. Bjorgo, S. P. D. Gill, et al., "A Comprehensive Analysis of Building Damage in the 12 January 2010 Mw7 Haiti Earthquake Using High-Resolution Satelliteand Aerial Imagery," Photogrammetric Engineering & Remote Sensing, vol. 77, pp. 997-1009, 2011.
[36] J. Tian, A. A. Nielsen, and P. Reinartz, "Building damage assessment after the earthquake in Haiti using two post-event satellite stereo imagery and DSMs," International Journal of Image and Data Fusion, vol. 6, pp. 155-169, 2015.
[37] H. Miura, S. Midorikawa, and M. Matsuoka, "Building Damage Assessment Using High-Resolution Satellite SAR Images of the 2010 Haiti Earthquake," Earthquake Spectra, 2015.
[38] Ehrlich, D., H. D. Guo, K. Molch, J. W. Ma, and M. Pesaresi. "Identifying Damage Caused by the 2008 Wenchuan Earthquake from VHR Remote Sensing Data." International Journal of Digital Earth 2 (December): 309–326, 2009.
[39] Chini, M., N. Pierdicca, and W. J. Emery. "Exploiting SAR and VHR Optical Images to Quantify Damage Caused by the 2003 Bam Earthquake." Geoscience and Remote Sensing, IEEE Transactions on 47: 145–152, 2009.
[40] Meslem, F. Yamazaki, and Y. Maruyama, "Accurate evaluation of building damage in the Boumerdes Algeria earthquake from Quickbird satellite image" Journal of Earthquake and Tsunami, vol. 05, pp. 1-18, 2011.
[41] M. Turker and B. Cetinkaya, "Automatic detection of earthquake-damaged buildings using DEMs created from pre- and post-earthquake stereo aerial photographs," International Journal of Remote Sensing, vol. 26, pp. 823-832, 2005.
[42] X. Tong, Z. Hong, S. Liu, X. Zhang, H. Xie, Z. Li, et al., "Building-damage detection using pre- and post-seismic high-resolution satellite stereo imagery: A case study of the May 2008 Wenchuan earthquake," ISPRS Journal of Photogrammetry and Remote Sensing, vol. 68, pp. 13-27, 2012.
[43] S. Stramondo, C. Bignami, M. Chini, N. Pierdicca, and A. Tertulliani, "Satellite radar and optical remote sensing for earthquake damage detection: results from different case studies," International Journal of Remote Sensing, vol. 27, pp. 4433-4447, 2006.
[44] Brunner, D., G. Lemoine, and L. Bruzzone. "Earthquake Damage Assessment of Buildings Using VHR Optical and SAR Imagery." Geoscience and Remote Sensing, IEEE Transactions on 48: 2403–2420, 2010.
[45] L. Gusella, B. J. Adams, G. Bitelli, C. K. Huyck, and A. Mognol, "Object-Oriented Image Understanding and Post-Earthquake Damage Assessment for the 2003 Bam, Iran, Earthquake," Earthquake Spectra, vol. 21, pp. 2005.
[46] D. Tiede, S. Lang, P. Füreder, D. Hölbling, C. Hoffmann, and P. Zeil, "Automated Damage Indication for Rapid Geospatial Reporting," Photogrammetric Engineering & Remote Sensing, vol. 77, pp. 933-942, 2011.
[47] P. Li, H. Xu, and J. Guo, "Urban building damage detection from very high-resolution imagery using OCSVM and spatial features," International Journal of Remote Sensing, vol. 31, pp. 3393-3409, 2010.
[48] Vetrivel, M. Gerke, N. Kerle, and G. Vosselman, "Identification of damage in buildings based on gaps in 3D point clouds from very high resolution oblique airborne images," ISPRS Journal of Photogrammetry and Remote Sensing, vol. 105, pp. 61-78, 2015.
[49] M. Gerke and N. Kerle, "Automatic Structural Seismic Damage Assessment with Airborne Oblique Pictometry© Imagery," Photogrammetric Engineering & Remote Sensing, vol. 77, pp. 885-898, 2011.
[50] Y. Maruyama, A. Tashiro, and F. Yamazaki, "Detection of Collapsed Buildings Due to Earthquakes Using a Digital Surface Model Constructed from Aerial Images," Journal of Earthquake and Tsunami, vol. 08, p. 1450003, 2014.
[51] C. Cao, D. Liu, R. P. Singh, S. Zheng, R. Tian, and H. Tian, "Integrated detection and analysis of earthquake disaster information using airborne data," Geomatics, Natural Hazards and Risk, pp. 1-30, 2015.
[52] Y. Dong, Q. Li, A. Dou, and X. Wang, "Extracting damages caused by the 2008 Ms 8.0 Wenchuan earthquake from SAR remote sensing data," Journal of Asian Earth Sciences, vol. 40, pp. 907-914, 2011.
[53] G. Trianni and P. Gamba, "Damage detection from SAR imagery: Application to the 2003 Algeria and 2007 Peru earthquakes," International Journal of Navigation and Observation, vol. 20, 2008.
[54] Y. Bazi, L. Bruzzone, and F. Melgani, "An unsupervised approach based on the generalized Gaussian model to automatic change detection in multitemporal SAR images," Geoscience and Remote Sensing, IEEE Transactions on, vol. 43, pp. 874-887, 2005.
[55] Z. Hong, X. Tong, W. Cao, S. Jiang, P. Chen, and S. Liu, "Rapid three-dimensional detection approach for building damage due to earthquakes by the use of parallel processing of unmanned aerial vehicle imagery," Journal of Applied Remote Sensing, vol. 9, pp. 097292-097292, 2015.
[56] J. Fernandez Galarreta, N. Kerle, and M. Gerke, "UAV-based urban structural damage assessment using object-based image analysis and semantic reasoning," Nat. Hazards Earth Syst. Sci., vol. 15, pp. 1087-1101, 2015.
[57] C. Parape, C. Premachandra, and M. Tamura, "Optimization of structure elements for morphological hit-or-miss transform for building extraction from VHR airborne imagery in natural hazard areas," International Journal of Machine Learning and Cybernetics, vol. 6, pp. 641-650, 2015.
[58] R. W. Conners, M. M. Trivedi, and C. A. Harlow, "Segmentation of a high-resolution urban scene using texture operators," Computer Vision, Graphics, and Image Processing, vol. 25, pp. 273-310, 1984.
[59] G. Taskin, O. K. Ersoy, and M. E. Kamasak, "Earthquake-induced damage classification from postearthquake satellite image using spectral and spatial features with support vector selection and adaptation," Journal of Applied Remote Sensing, vol. 9, pp. 096017-096017, 2015.
[60] F. Yamazaki, Y. Yano, and M. Matsuoka, "Visual Damage Interpretation of Buildings in Bam City Using QuickBird Images Following the 2003 Bam, Iran, Earthquake," Earthquake Spectra, vol. 21, pp. 329-336, 2005.
[61] M. Hill and T. Rossetto, "Comparison of building damage scales and damage descriptions for use in earthquake loss modelling in Europe," Bulletin of Earthquake Engineering, vol. 6, pp. 335-365, 2008.
[62] M. Dolce and A. Goretti, "Building damage assessment after the 2009 Abruzzi earthquake," Bulletin of Earthquake Engineering, vol. 13, pp. 2241-2264, 2015.
[63] J. Schwarz, L. Abrahamczyk, M. Leipold, and T. Wenk, "Vulnerability assessment and damage description for R.C. frame structures following the EMS-98 principles," Bulletin of Earthquake Engineering, vol. 13, pp. 1141-1159, 2015.
[64] N. Kerle, "Satellite-based damage mapping following the 2006 Indonesia earthquake—How accurate was it?" International Journal of Applied Earth Observation and Geoinformation, vol. 12, pp. 466-476, 2010.
[65] F. De Luca, G. Verderame, and G. Manfredi, "Analytical versus observational fragilities: the case of Pettino (Lâ€™Aquila) damage data database," Bulletin of Earthquake Engineering, vol. 13, pp. 1161-1181, 2015.
[66] K. Goda, T. Kiyota, R. Pokhrel, G. Chiaro, T. Katagiri, K. Sharma, et al., "The 2015 gorkha nepal earthquake: insights from earthquake damage survey," Name: Frontiers in Built Environment, vol. 1, 2015.
[67] M. Okamura, N. P. Bhandary, S. Mori, N. Marasini, and H. Hazarika, "Report on a reconnaissance survey of damage in Kathmandu caused by the 2015 Gorkha Nepal earthquake," Soils and Foundations, 2015.
[68] G. Chiaro, T. Kiyota, R. M. Pokhrel, K. Goda, T. Katagiri, and K. Sharma, "Reconnaissance report on geotechnical and structural damage caused by the 2015 Gorkha Earthquake, Nepal," Soils and Foundations, 2015.
[69] Angster, Stephen, Eric J. Fielding, Steven Wesnousky, Ian Pierce, Deepak Chamlagain, Dipendra Gautam, Bishal Nath Upreti, Yasuhiro Kumahara, and Takashi Nakata. "Field Reconnaissance after the 25 April 2015 M 7.8 Gorkha Earthquake." Seismological Research Letters 86: 1506–1513, 2015.
[70] L. Ge, A. H.-M. Ng, X. Li, Y. Liu, Z. Du, and Q. Liu, "Near real-time satellite mapping of the 2015 Gorkha earthquake, Nepal," Annals of GIS, vol. 21, pp. 175-190, 2015.
[71] Breiman, Leo. "Random Forests." Machine Learning 45: 5–32, 2001.
[72] G. Grünthal, European macroseismic scale 1992: updated MSK scale vol. 7: European Seismological Commission, Subcommission on Engineering Seismology, Working Group Macroseismic scale, 1993.
[73] Cohen, J. "A Coefficient of Agreement for Nominal Scales." 3. Educational and Psychological Measurement 20 (1): 37–46, 1960.